OCEANOGRAPHY

Rapid Red Sea Deep Water renewals caused by volcanic eruptions and the North Atlantic Oscillation

Fengchao Yao[1]* and Ibrahim Hoteit[2]*

The Red Sea hosts a deep marine environment unique among the world's oceans. It is occupied, almost homogeneously from the subsurface (~137 to 300 m) to depths over 2000 m, by a warm (~21.5°C) and highly saline (~40.5) water mass, referred to as the Red Sea Deep Water (RSDW). Previous studies suggested that the RSDW is mainly ventilated, continuously or intermittently, by dense outflows from the northern Gulfs of Suez and Aqaba with a resulting sluggish renewal time on the order of 36 to 90 years. We use six repeated hydrographic observations spanning the period 1982–2011 and simulations of an ocean general circulation model with realistic atmospheric forcing to show that large portions of the RSDW were episodically replaced during 1982–2001 by new dense waters mainly formed by open-ocean deep convections in the northern Red Sea during anomalously cold winters, pointing to a much shorter renewal time for the RSDW on the order of a decade. We further show that the winter cooling anomaly in the Red Sea region was a part of a large-scale climate variability pattern associated with either large volcanic eruptions or the North Atlantic Oscillation (NAO). Consequently, significant deep water formation events occurred in the Red Sea in the winters following the 1982 El Chichón eruption in Mexico and the 1991 Mount Pinatubo eruption in the Philippines and during the strong positive phase of the NAO in the winter of 1989.

INTRODUCTION

The Red Sea is an elongated, semi-enclosed marginal sea of the Indian Ocean (fig. S1). The deep basin (>2000 m) and shallow connection (137 m) through the Strait of Bab el Mandeb to the Indian Ocean leads to a two-cell vertical overturning circulation system in the Red Sea (1). A shallow overturning cell, consisting of an annual mean northward surface inflow and a southward intermediate outflow, lies above the sill depth in the south and deepens to about 300 m in the north. Directly subject to the annual cycle of surface heat flux and excessive surface fresh water loss (~2 m/year), this overturning cell is characterized by marked seasonal temperature variations and a northward increase in salinity in the upper branch and is sustained by the winter formation of the Red Sea intermediate water, which is then exported into the Indian Ocean through the Strait of Bab el Mandeb (2, 3). In contrast, below the shallow cell (~137 to 300 m) and extending to depths >2000 m, the Red Sea is horizontally blocked from direct water exchanges with the Indian Ocean by the sill in the strait and is occupied by a nearly homogeneous warm (~21.5°C) and highly saline (~40.5) water mass, referred to as the Red Sea Deep Water (RSDW). Nevertheless, a deep overturning cell is manifested by the gradients in the distributions of geochemical tracers and dissolved oxygen in the RSDW. The circulation pattern of the deep cell inferred from the tracers consists of an injection of dense deep water into the northern Red Sea, a southward bottom current, and a northward returning current, at depths of 400 to 600 m (1, 4–6).

Because the formation processes of the dense deep water, the key driver for the deep overturning cell in the Red Sea and the RSDW renewal, were poorly constrained by the sparse data available for the Red Sea, the rates and mechanisms of the renewal of the RSDW remain

mainly speculative and largely uncertain. Estimates suggest that renewal time of the RSDW is sluggish, and on the order of 36 to 90 years (1, 4, 7). Furthermore, the above pattern of the deep overturning cell was inferred from a few synoptic observations and only represented a snapshot view of the deep circulation without resolving the temporal evolutions of the process. Woelk and Quadfasel (7) used three hydrographic sections collected in 1982, 1983, and 1987 along the major axis of the basin to show the intermittent nature of the RSDW's renewal process. They identified one significant episode of deep water formation in the winter of 1982–1983 under anomalously cold conditions. Observations suggest that the large-scale climate variability associated with large tropical volcanic eruptions or the North Atlantic Oscillation (NAO) (8) can lead to anomalously cold conditions during winters in the Middle East (9–11). However, the relationship between these climate variabilities and the renewal processes of RSDW has not yet been explored. Here, we present hydrographic observations to show that large portions of the RSDW were intermittently renewed during the period 1982–2001 by episodic deep water formation events, which suggests that renewal time for the RSDW is on the order of a decade rather than 36 to 90 years. We then use simulations from an ocean general circulation model to elucidate that the deep water formation processes are, in fact, an oceanic response to large volcanic eruptions and strong positive NAO.

RESULTS

Hydrographic observations

Conductivity-temperature-depth (CTD) measurements along the central axis of the Red Sea collected from six cruises in 1982, 1983, 1987, 1995, 2001, and 2011 (see Materials and Methods) reveal distinctive interannual-to-decadal changes in the deep water temperatures (Fig. 1) and salinities (fig. S2), providing direct observational evidence that the RSDW was renewed episodically at a rapid pace during the period 1982–2001. The observations in 1982, 1983, and 1987, as reported in a previous study (7), depict a deep water renewal episode, in which colder, fresher water was formed in the north

[1]King Abdullah University of Science and Technology, Biological and Environmental Science and Engineering Division, Thuwal 23955-6900, Saudi Arabia. [2]King Abdullah University of Science and Technology, Physical Science and Engineering Division, Thuwal 23955-6900, Saudi Arabia.
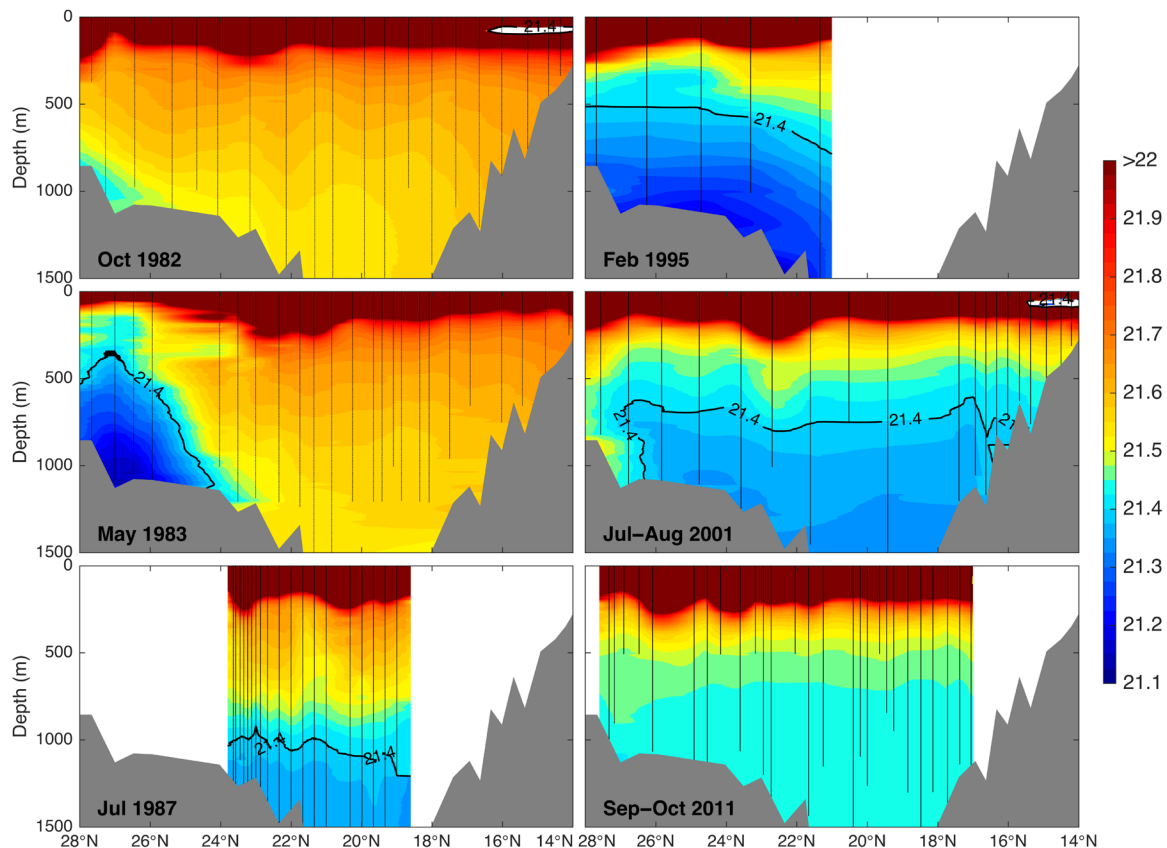*Corresponding author. Email: fengchao.yao@kaust.edu.sa (F.Y.); Ibrahim.hoteit@kaust.edu.sa (I.H.)

Fig. 1. Sections of potential temperature (°C) along the central axis in the Red Sea collected in 1982, 1983, 1987, 1995, 2001, and 2011. The dotted vertical lines mark the locations of the CTD profiles, and regions without observations are left blank. The color map in the range of 21.1° to 22°C is chosen to highlight the changes and structures of the deep water.

during the 1982–1983 winter and, after spreading southward, filled the central basin below 1000 m in 1987. For simplicity, the new deep water in this study is defined as the waters colder than 21.4°C. The more recent observations in 1995, 2001, and 2011 indicate that one or multiple deep water formation events also occurred between 1987 and 1995, as evidenced by the newly formed colder and fresher deep water present below 500 m in the 1995 observations. Although the 1995 observations were limited to north of 21°N, it is evident that the deep water formed during 1987–1995 was much larger in volume than that formed in the winter of 1982–1983. As a result, the new deep water replaced a much larger portion of the old deep water afterward and still filled the entire basin below 700m in 2001. Note that, as the deep water was periodically cooled by the newly formed water in the north, it was also constantly warmed through vertical diffusion by the upper water, which is directly influenced by surface heat flux. The new deep water returned to a relative warm state in the 2011 observations, implying that no significant deep water formation events occurred during the period 2001–2011.

Model results

To explore the physical processes and to pinpoint the timing of the deep water formation events observed in the Red Sea and their relationship to external atmospheric conditions, we ran a high-resolution Massachusetts Institute of Technology general circulation model (MITgcm) (12) simulation for the period 1979–2001. The horizontal

resolution of the model was about 1.5 km, and the model domain included the Gulf of Aqaba and the Gulf of Suez, both connected to the northern end of the Red Sea. The model was forced by the realistic atmospheric reanalysis data set produced by the European Center for Medium Range Weather Forecasts [ERA-Interim, (13)], which assimilates the global archived observations and provides climate variability in the atmospheric conditions (see Materials and Methods for the detailed configurations). The configurations of the model have been used successfully to study the shallow seasonal overturning circulation (3, 14). Moreover, the seasonal and interannual variability in the modeled sea surface temperatures agree well with results from the observation-based Optimum Interpolation Sea Surface Temperature [OISST; see Materials and Methods (15)] during the period 1982–2001 (Fig. 2).

The model simulation further reveals a full series of deep water formation events that episodically injected colder, fresher waters into the deep basin of the northern Red Sea (Fig. 3A and fig. S3). The abrupt transitions of cooling and freshening in the time series of the temperature and salinity vertical profiles (Fig. 3A and fig. S3) and the accompanying increases in the volume of the newly produced deep water, calculated as the summation of the deep water with potential temperatures less than 21.4°C (Fig. 3B), allowed us to identify four major deep water formation events that occurred in the late winters of 1983, 1989, 1992, and 1993. The timing of the modeled events, particularly the 1983 winter event that
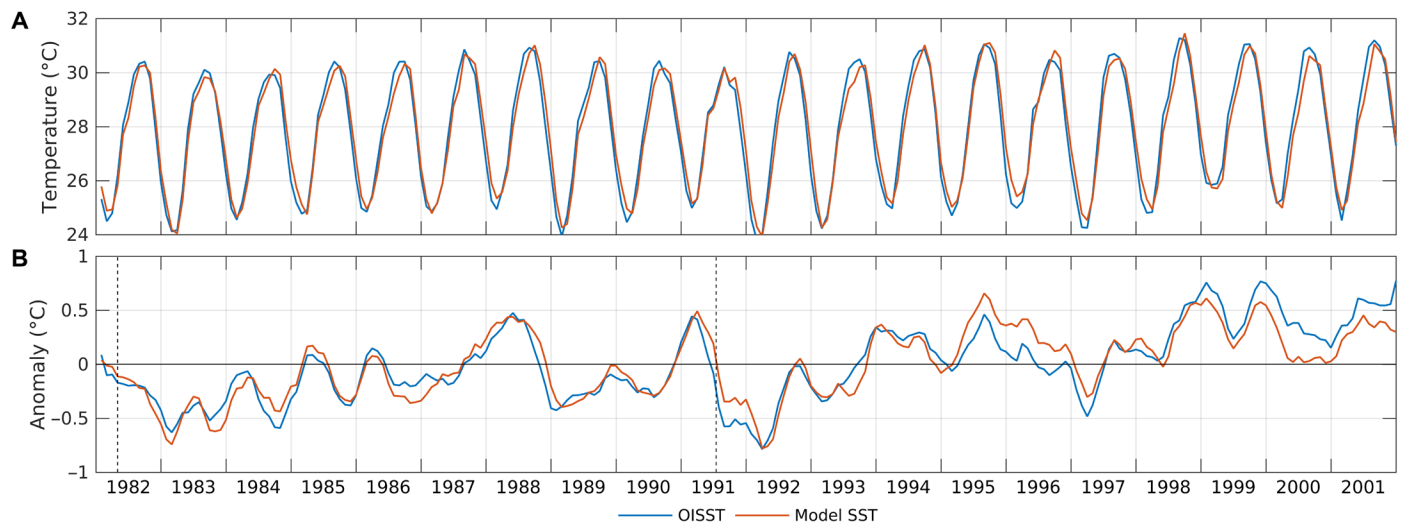
Fig. 2. Comparisons of the seasonal and interannual variability between the modeled and observed sea surface temperatures. (**A**) Monthly means and (**B**) monthly anomalies for the basin averaged sea surface temperatures derived from the MITgcm simulation and OISST. The monthly anomalies are relative to the 1982–2001 monthly climatological means, and 5-month moving averaging is applied. The dashed lines indicate the 1982 El Chichón and 1991 Mount Pinatubo eruptions.

was pinpointed by the observations, are consistent with the observed deep water changes shown in Fig. 1. Moreover, the modeled deep water formation events lead to changes in temperature and salinity in the deep water (fig. S4) that match the corresponding observations shown in Fig. 1, indicating that the volumes of the deep water produced by these events were also realistically reproduced in the model.

Three sources, including deep outflows from the Gulf of Suez and the Gulf of Aqaba and open-ocean deep convection in the northern Red Sea, have long been proposed for the formation of the RSDW (16). Previous studies focused on the importance of the Suez and Aqaba outflows in the formation of the RSDW (1, 7, 17, 18). The outflow from the Gulf of Suez, where the densest water in the whole basin is normally formed during winters because of the higher latitudes and shallow water depths (with a maximum depth of 70 m), was invoked as the sole source of deep water to explain the observed deep water changes between 1982 and 1983 (7). The outflow from the Gulf of Aqaba, a much deeper basin than the Gulf of Suez (with a maximum depth of 1850 m), was suggested by observed chlorofluorocarbon distributions to have contributed to the formation of the bottom water of the Red Sea (17).

Contrary to these studies, our model results indicate that the open-ocean deep convection in the northern Red Sea, usually considered as an unlikely source because of the lack of direct observations, is the primary source for the RSDW formation during the period 1982–2001, whereas the outflows from the Gulfs of Suez and Aqaba act collectively as the secondary sources. The deep convection and the outflows each contribute to the deep water formation through distinct dynamical processes and pathways as schematically shown in fig. S5; in the following paragraph, their mechanisms are briefly described and their respective annual contributions to the deep water formation are estimated from the model results.

Deep convection episodes occurring in the interior of the basin are indicated from the bottom-reaching penetrations of the surface mixed layer in the time series of temperature profiles during the deep water formation events, implicating the conditions of intense

surface heat loss from the sea to the air (Fig. 3A). At the same time, the deep convections reduces the salinity in the deep water because of vertical mixing with the fresher water in the upper layer (fig. S3). The physical process of the deep convection in the northern Red Sea differs significantly from the other deep convection sites in the world ocean, such as the Labrador Sea and the northwestern Mediterranean, where the deep convection occurs inside a cyclonic circulation that forms a doming of the density surface and creates a favorable precondition for the convection (19). Although a winter cyclonic circulation is normally present in the northern Red Sea (3), the deep convection in each event in the model starts along the western coast between 26°N and 27°N and laterally develops into the interior of the basin. The surface temperatures and regions of the deep convection during the peak stage in each event, when the deep convection regions reached the maximum surface area in February or March, are displayed in Fig. 4. The deep convection region, in which the surface mixed layer depths reach the bottom, is diagnosed as the area where the density difference between the surface and the bottom is less than 0.1 kg/m^3. Depending on the intensities of the atmospheric forcing and details of the circulation, the areas and shapes of the deep convection region during the peak stage vary markedly in different years, but the coldest surface waters in all the events are generally collocated with the deep convection regions and tend to be located at the western side of the basin. The locations of the deep convection regions are consistent with the patterns associated with the upper overturning circulation (3), in which the isotherms tilt upward along the western coast because of upwelling in every winter, thus reducing the vertical stratification there and setting up favorable preconditions for the open-ocean deep convections to take place.

The Gulfs of Suez and Aqaba contribute to the RSDW through bottom-trapped density outflows that follow dynamical processes similar to that of the well-studied overflows, such as the Red Sea overflow into the Gulf of Aden and Mediterranean overflow into the Atlantic (20). The overflows from the gulfs accelerate initially because of density differences after exiting the source region, veer
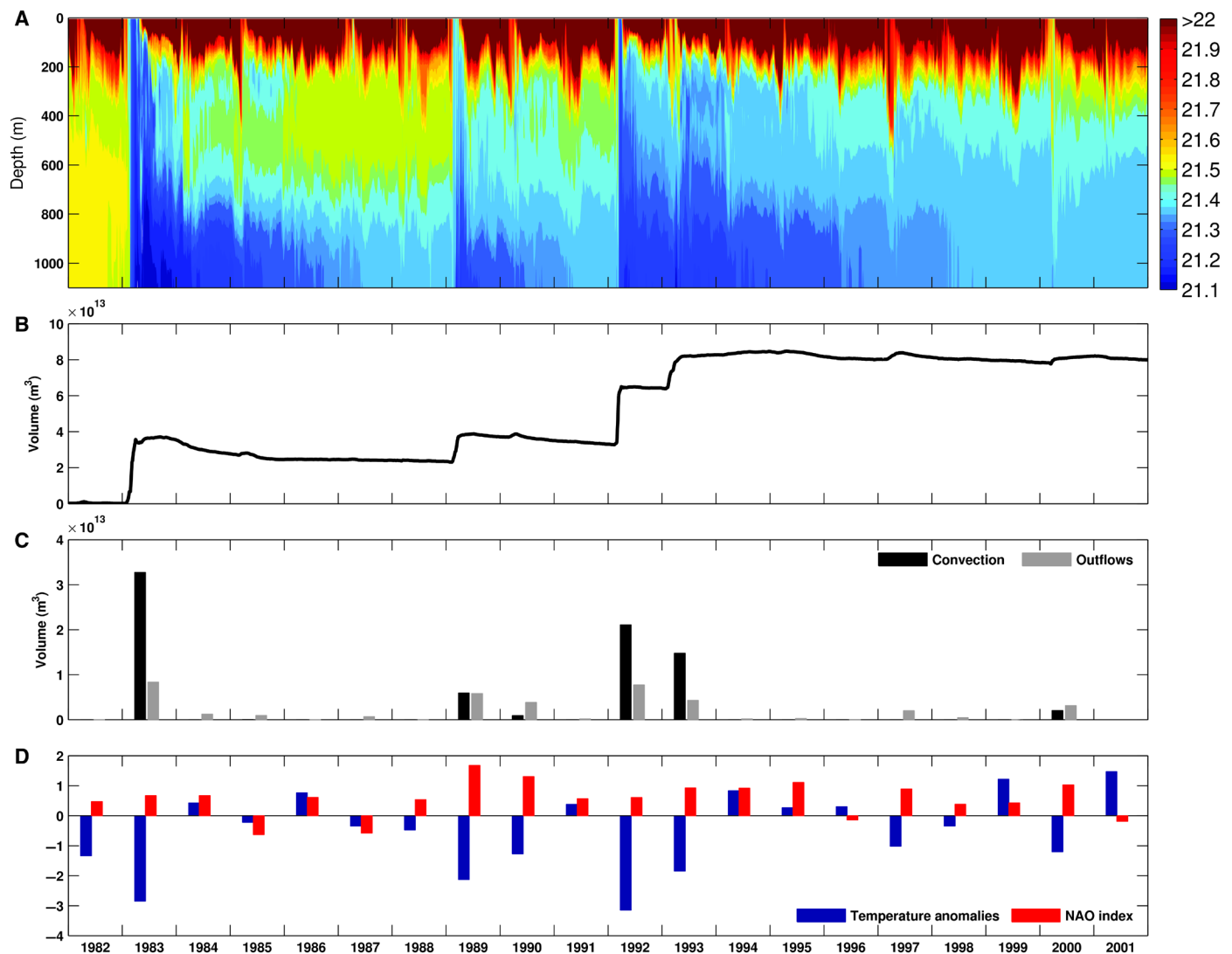
Fig. 3. Deep water formation events during the period 1982–2001. (**A**) Time series of modeled vertical temperature profiles in the northern Red Sea (34.6°E, 27.2°N; see fig. S1 for the locations). (**B**) Changes in the volumes of the new deep water with potential temperatures lower than 21.4°C. (**C**) Annual contributions from the open-ocean deep convection and combined outflows from the Gulfs of Suez and Aqaba to the deep water formation. (**D**) Winter (January through March) surface air temperature anomalies normalized by the 1951–1980 SD in the northern Red Sea (see fig. S1 for the location) and the corresponding winter (January through March) NAO indices.

to the right of the flow direction because of geostrophy, and experience significant dilutions and increases in volume due to entrainment with the ambient waters. Depending on the properties of the source waters, the final product waters can either reach neutral density and spread at intermediate depths or remain dense enough to sink to the deep layer. These processes are illustrated by a downstream section using the 1983 event as an instance (Fig. 5). Initially, in January 1983, the outflows behave similarly to those during the normal winter conditions and are not dense enough to sink to the deep part of the basin; they appear as relatively warm and salty southward subsurface flows banking against the western side of the coast at depths between 100 and 500 m. Later, in February 1983, under the abnormal winter cooling conditions in 1983, the source waters in the gulfs become much colder and denser, and the outflows, even after substantial dilutions by entrainment with ambient waters, reach the bottom of the northern Red Sea. While the peak stage of the deep

convection occurs in March and lasts a relatively short time period of less than 1 month, the outflows continuously inject cold waters to the deep part of the basin from February to May, which remain noticeable in May 1983 during the restratification stage after the open-ocean deep convection.

The respective annual contributions from deep convections and outflows to the deep water are displayed in Fig. 3C (see Materials and Methods for the calculation of the annual contributions). It can be seen that the deep convections were the dominant contributors to the deep water formations during the three largest events in 1983, 1992, and 1993. The volume of the deep water formation estimated in the model for 1983 is more consistent with these observations than that estimated from a one-dimensional plume model that includes only the outflow from the Gulf of Suez (7). The total volume of the deep water formation in 1983 from the model, including both contributions from the deep convection and the outflows, is about 4.0×10^{13} m^3 (Fig. 3C),
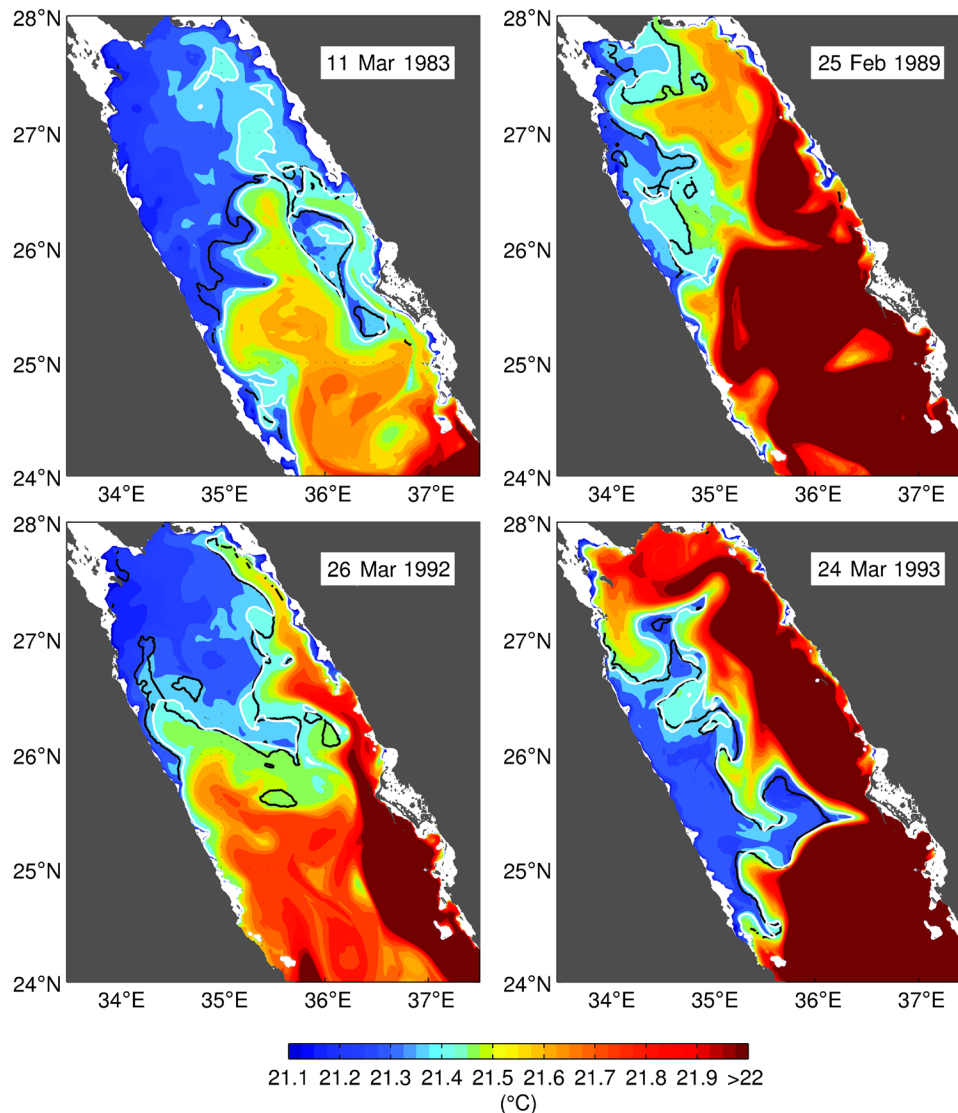
Fig. 4. Modeled sea surface temperatures and deep convection regions during the peak stages in the deep water formation years. The dates refer to the middle day of the 3-day averaged model outputs. The deep convection regions are diagnosed as the area where the density difference between the surface and the bottom is less than 0.1 kg/m^3 and are separated from the nondeep-convection regions by the black lines. The 21.4°C isotherms are marked by the white lines. The deep convection regions are generally collocated with cold waters and tend to be at the western side of the basin.

the plume model yields a volume of 1.0×10^{13} m^3 (a formation rate of 0.58×10^6 m^3/s over a period of 7 months), and the 1983 observation in Fig. 1 yields an estimate of the volume of 3.6×10^{13} m^3 (assuming a uniform distribution of water properties across the basin and that the width of the basin, axial length, and thickness of the new deep water are 200 and 450 km and 800 m, respectively). Therefore, to reproduce the observed formation of deep water in 1983, the deep convection in the northern Red Sea must have occurred as a deep water source that prevails over the outflows from the gulfs.

Links between the RSDW renewals and volcanic eruptions and the NAO

The timing of the major deep water formation events in 1983, 1989, 1992, and 1993, as determined by the model, is linked with the observed anomalously cold winters over the northern Red Sea (Fig. 3D). The effects of volcanic eruptions and NAO on the northern Red Sea

are apparent by the low surface air temperatures (see Materials and Methods for the data source) in the winter of 1989, which was in a strong positive NAO phase, and in the winters of 1983, 1992, and 1993, which fell within the winters following the 1982 El Chichón eruption in Mexico and the 1991 Mount Pinatubo eruption in the Philippines, the two largest volcanic eruptions during the period 1982–2001.

The spatial structure of the averaged atmospheric circulation during the winters when the deep water formation event occurred (1983, 1989, 1992, and 1993) suggests that the anomalous cooling winter conditions in the Red Sea region were part of the large-scale climate fluctuations shown in the composite maps of the surface air temperature, sea-level pressure, and surface wind anomalies (Fig. 6A). The characteristic pattern during a positive NAO emerges in the anomaly maps, including a pattern of warming in Europe and cooling in the Middle East, an enhanced westerly zonal jet stream
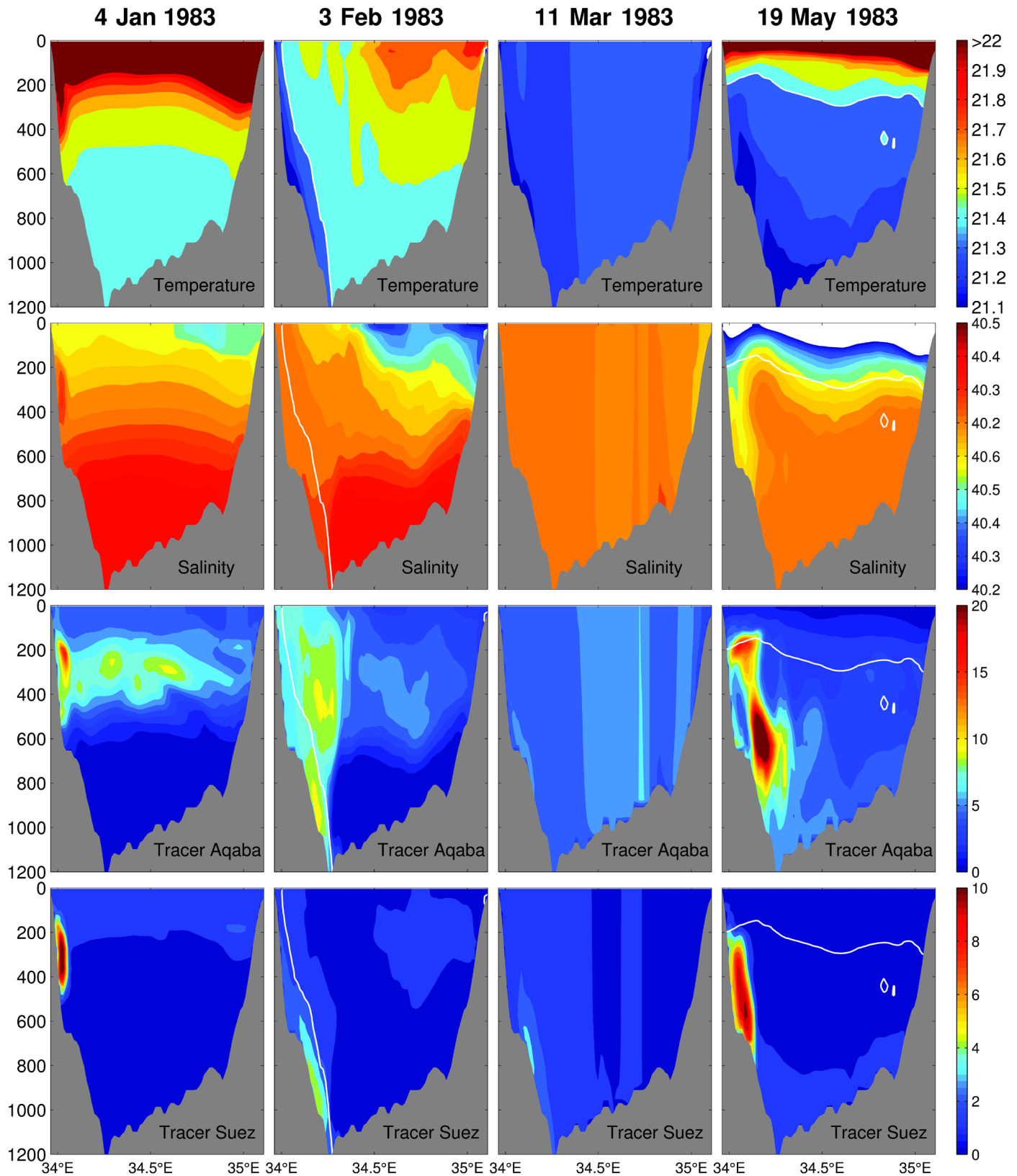
Fig. 5. Contributions from the outflows to the RSDW in the 1983 winter as illustrated by the potential temperature, salinity, and tracer sections located at the downstream of the outflows. The dates are referring to the middle day of the 3-day averaged model outputs. See fig. S1 for the location of the section in the Red Sea. The overflows from the Gulfs of Suez and Aqaba are tagged with tracers. The 21.4°C contours of the potential temperature are also plotted as white lines in each section when present.
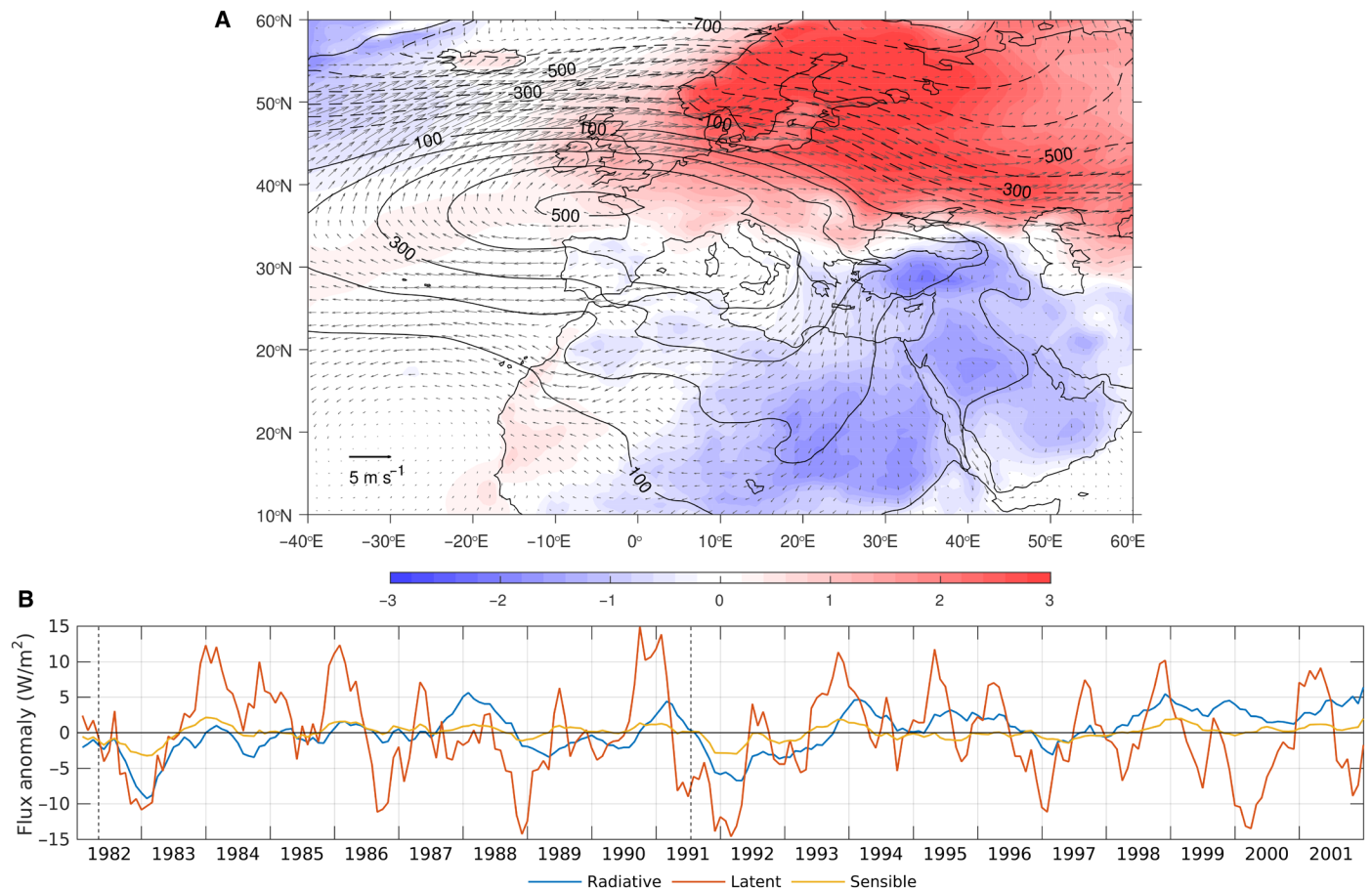
Fig. 6. Surface heat flux anomalies for the deep water formation events. (**A**) Composite maps of winter (January through March) anomalies of the surface wind (vectors), temperature (shadings), and sea-level pressure (contours) during the deep water formation years (1983, 1989, 1992, and 1993) derived from the ERA-Interim reanalysis data. The anomalies are relative to the 1982–2001 monthly climatological mean. (**B**) Monthly anomalies for the basin-averaged radiative, latent, and sensible heat fluxes from the model results. Positive value indicates heat gain by the Red Sea. The radiative flux is the net downward flux of the short- and long-wave radiative fluxes. The monthly anomalies are relative to the 1982–2001 monthly climatological means, and 5-month moving averaging is applied. The vertical dashed lines indicate the 1982 El Chichón and 1991 Mount Pinatubo eruptions.

across the Atlantic and an anticyclonic high sea-level pressure anomaly centered at western Europe. Located at the southeastern edge of this pressure anomaly pattern, the Red Sea experienced significantly intensified winter surface latent and sensible heat losses during these deep water formation years (Fig. 6B), due to the enhanced northwesterly surface winds that carried cold and dry continental air over the basin.

While the NAO is the dominant mode of inherent atmospheric variability in the north Atlantic sector, large volcanic eruptions also tend to trigger positive NAOs in the following winters (*21*). During a large volcanic eruption, an enormous amount of sulfate aerosols is injected into the atmosphere, resulting in a significant warming in the tropical stratosphere. This warming subsequently strengthens the equator-to-pole pressure gradient and increases the wind speeds of the zonal jet stream across the Atlantic, leading to an atmospheric fluctuation pattern resembling that of a positive NAO. Large volcanic eruptions can thus affect atmospheric conditions over the Red Sea during winter through a similar dynamical mechanism to a positive NAO. However, the model results suggest that significantly higher volumes of deep water were formed in the winters of 1983, 1992, and 1993 following large volcanic eruptions than in the winter of

1989 when the strongest positive NAO occurred during the period 1982–2001. These differences can be attributed to the additional cooling effects of the volcanic eruptions on the radiative fluxes (*22*). Following the injections of sulfate aerosol by the eruptions in April 1982 and June 1991, the net downward radiative flux reaching the sea surface was reduced for 1 or 2 years (Fig. 6B), and the sea surface temperatures averaged over the Red Sea exhibited marked cold anomalies (Fig. 2B), creating more favorable initial conditions for the deep water formation events during the following winters.

DISCUSSION
We used in situ hydrographic observations and a high-resolution general circulation model simulation to show that the Red Sea deep circulation is dictated by the large-scale climate variability associated with large volcanic eruptions and the NAO, translating these short-term fluctuations of the global climate into decadal changes in the deep water properties in the Red Sea through deep water formation processes. Two types of physical processes contributed to the deep water formations: the open-ocean deep convection in the

northern Red Sea and the outflows from the Gulfs of Suez and Aqaba, the former being the overall dominant one during the rapid RSDW renewals in the period 1982–2001. Although large volcanic eruptions tend to induce dynamical responses in the atmosphere over the Red Sea region that resembles a positive NAO, they have greater effects on the deep water formation processes than the NAO has because of the additional cooling from the direct radiative fluxes. The dynamic processes associated with the renewal of RSDW have profound effects on the Red Sea's ecosystem. Deep convection in the Red Sea leads to oxygenation of the deep water and to upward transport of nutrients from deep waters to the surface waters; subsequent southward propagation of the new dense water can also bring the deep nutrients closer to the surface at a basin-wide scale through the uplifting of the old deep water.

For wider implications, the responses of the RSDW to volcanic eruptions and the NAO are instrumental to examination of the influences of such climate variability on the global thermocline circulation. Global climate model simulations have shown that volcanic eruptions and the NAO act as the external drivers for the multidecadal variability of the Atlantic ocean circulations through their influences on the Atlantic Meridional Overturning Circulation (23–25), but the climate models suffer a great deal of divergences in the simulated results, partly due to their coarse resolutions, which do not resolve the relevant oceanic processes on the global scale. The Red Sea is often considered to be a miniature version of the world's ocean in that important dynamical processes in the global thermohaline circulation, such as the deep water formation from deep convection and overflows and the meridional overturning circulation, are present in the Red Sea (3). Owing to the small size and relatively simple shape of the basin, repeated observations and high-resolution modeling studies of the Red Sea are feasible. The observational and modeling results presented in this study provides a well-defined case on the responses of the deep circulation to volcanic eruptions and the NAO and may shed light on the understanding of the global effects of volcanic eruptions and the NAO.

MATERIALS AND METHODS
Hydrographic observations
The temperature and salinity data used in the analysis were collected on cruises carried out in October 1982 on the R/V *Marion Dufresne*, May 1983 on the R/V *Sagar Kanya*, July to August 1987 and February 1995 on the R/V *Meteor*, August 2001 on the R/V *Maurice Ewing*, and September to October 2011 on the R/V *Aegaeo*. The temperature and salinity were measured with CTD instruments, and the accuracies of the measurements were at least 0.02°C for temperature and 0.02 for salinity.

Model configurations
The model domain contained the Red Sea, the Gulf of Aqaba, the Gulf of Suez, and the western part of the Gulf of Aden. The model grids were defined on curvilinear coordinates rotated to align approximately with the major axis of the Red Sea. The model had a horizontal grid size of about 1.5 km and 40 vertical levels with layer thickness varying from 10 m in the surface to 100 m close to the deepest bottom. The model was forced with the 6-hourly ERA-Interim global climate reanalysis data, which are available from 1979 to date. Although the forecast model in the ERA-Interim uses climatological distributions of the aerosols and does not account explicitly for the variability of the aerosols caused by volcanic eruptions, the impacts of

volcanic aerosols on the atmospheric state are incorporated in the EAR-Interim reanalysis through assimilation of various satellite radiance data (26, 27). The open boundary conditions derived from the global ocean reanalysis data produced by the German partner of the consortium for Estimating the Circulation and Climate of the Ocean [GECCO, (28)], were prescribed in the eastern boundary of the domain in the Gulf of Aden. The model was run from 1979 to 2001, and 3-day averaged outputs were used in the analysis in this study. To track and distinguish the outflows from the Gulfs of Aqaba and Suez, passive tracers were released in the two gulfs, respectively, by relaxing to a fixed value of 100.

Optimum Interpolation Sea Surface Temperature
Defined on 1° grid, the OISST data set is a sea surface temperature analysis constructed from satellite, ship, and buoy measurements with bias adjustments applied. The monthly version of the data was used in this study. The data are publicly available at www.esrl.noaa.gov/psd/data/gridded/data.noaa.oisst.v2.html.

Surface air temperature anomalies
The monthly surface temperature anomaly data were derived from the Goddard Institute for Space Studies Surface Temperature Analysis (29). The data set is defined on a 2° × 2° grid. These surface air temperature anomalies represent large-scale patterns, since anomalies are obtained by weighted averaging of neighboring meteorological stations within 1200 km. The temperature anomalies are relative to the 1951–1980 mean and normalized by the SD of the same period. The data are publicly available at https://data.giss.nasa.gov/gistemp/.

Annual contributions to the deep water
The contribution from the deep convection in each year was calculated as the volume of the water column when the maximum surface area with temperatures less than 21.4°C is reached, as shown in Fig. 4, less the dense water already present in that water column. The contribution from the outflows was integrated from the velocities crossing the sections in Fig. 5 for the overflows that fulfill two conditions: First, the Aqaba or the Suez tracer concentration is larger than a threshold value of 5, and second, the potential temperatures are less than 21.4°C. Since the overall production rates from the two gulfs are relatively small compared with the production rate from the deep convection, the combined contributions from the two gulfs are shown in Fig. 3C.

The NAO index
The NAO index data used in Fig. 3D were downloaded from www.cpc.ncep.noaa.gov/products/precip/CWlink/pna/nao.shtml. The calculation of the NAO index is based on rotated principal component analysis of the 1950–2000 National Centers for Environmental Prediction reanalysis data.

SUPPLEMENTARY MATERIALS
Supplementary material for this article is available at http://advances.sciencemag.org/cgi/content/full/4/6/eaar5637/DC1

fig. S1. The bathymetry of the Red Sea.
fig. S2. Sections of salinity along the central axis in the Red Sea collected in 1982, 1983, 1987, 1995, 2001, and 2011.
fig. S3. Time series of modeled vertical salinity profiles in the northern Red Sea.
fig. S4. Axial potential temperature sections plotted from the model results for comparing with the corresponding observed sections in Fig.1.
fig. S5. Schematic of deep water formation in the northern Red Sea from three different sources.

REFERENCES AND NOTES

1. R. P. Cember, On the sources, formation, and circulation of Red Sea Deep Water. *J. Geophys. Res.* **93**, 8175–8191 (1988).

2. E. Tragou, C. Garrett, The shallow thermohaline circulation of the Red Sea. *Deep Sea Res. Part I Oceanogr. Res. Pap.* **44**, 1355–1376 (1997).

3. F. Yao, I. Hoteit, L. J. Pratt, A. S. Bower, A. Köhl, G. Gopalakrishnan, D. Rivas, Seasonal overturning circulation in the Red Sea: 2. Winter circulation. *J. Geophys. Res.* **119**, 2263–2289 (2014).

4. G. Eshel, M. A. Cane, M. B. Blumenthal, Modes of subsurface, intermediate, and deep water renewal in the Red Sea. *J. Geophys. Res.* **99**, 15941–15952 (1994).

5. P. Jean-Baptiste, E. Fourré, N. Metzl, J. F. Ternon, A. Poisson, Red Sea deep water circulation and ventilation rate deduced from the ^{3}He and ^{14}C tracer fields. *J. Mar. Syst.* **48**, 37–50 (2004).

6. S. S. Sofianos, W. E. Johns, Observations of the summer Red Sea circulation. *J. Geophys. Res.* **112**, C06025 (2007).

7. S. Woelk, D. Quadfasel, Renewal of deep water in the Red Sea during 1982–1987. *J. Geophys. Res.* **101**, 18155–18165 (1996).

8. J. W. Hurrell, Decadal trends in the North-Atlantic Oscillation: Regional temperatures and precipitation. *Science* **269**, 676–679 (1995).

9. A. Robock, J. Mao, Winter warming from large volcanic eruptions. *Geophys. Res. Lett.* **19**, 2405–2408 (1992).

10. A. Genin, B. Lazar, S. Brenner, Vertical mixing and coral ceath in the Red-Sea following the eruption of Mount Pinatubo. *Nature* **377**, 507–510 (1995).

11. N. Rimbu, G. Lohmann, T. Felis, J. Pätzold, Arctic oscillation signature in a Red Sea coral. *Geophys. Res. Lett.* **28**, 2959–2962 (2001).

12. J. Marshall, C. Hill, L. Perelman, A. Adcroft, Hydrostatic, quasi-hydrostatic, and nonhydrostatic ocean modeling. *J. Geophys. Res.* **102**, 5733–5752 (1997).

13. D. P. Dee, S. M. Uppala, A. J. Simmons, P. Berrisford, P. Poli, S. Kobayashi, U. Andrae, M. A. Balmaseda, G. Balsamo, P. Bauer, P. Bechtold, A. C. M. Beljaars, L. van de Berg, J. Bidlot, N. Bormann, C. Delsol, R. Dragani, M. Fuentes, A. J. Geer, L. Haimberger, S. B. Healy, H. Hersbach, E. V. Hólm, L. Isaksen, P. Kållberg, M. Köhler, M. Matricardi, A. P. McNally, B. M. Monge-Sanz, J.-J. Morcrette, B.-K. Park, C. Peubey, P. de Rosnay, C. Tavolato, J.-N. Thépaut, F. Vitart, The ERA-Interim reanalysis: Configuration and performance of the data assimilation system. *Q. J. R. Meteorol. Soc.* **137**, 553–597 (2011).

14. F. Yao, I. Hoteit, L. J. Pratt, A. S. Bower, P. Zhai, A. Köhl, G. Gopalakrishnan, Seasonal overturning circulation in the Red Sea: 1. Model validation and summer circulation. *J. Geophys. Res.* **119**, 2238–2262 (2014).

15. R. W. Reynolds, N. A. Rayner, T. M. Smith, D. C. Stokes, W. Wang, An improved in situ and satellite SST analysis for climate. *J. Climate* **15**, 1609–1625 (2002).

16. K. Wyrtki, On the deep circulation of the Red Sea, in *Processus de formation des Eaux Océaniques Profondes* (Colloques Internationaux du CNRS, No. 215, 1974), pp. 91–106.

17. O. Plähn, B. Baschek, T. H. Badewien, M. Walter, M. Rhein, Importance of the Gulf of Aqaba for the formation of bottom water in the Red Sea. *J. Geophys. Res.* **107**, 22-1–22-18 (2002).

18. V. P. Papadopoulos, P. Zhan, S. S. Sofianos, D. E. Raitsos, M. Qurban, Y. Abualnaja, A. Bower, H. Kontoyiannis, A. Pavlidou, T. T. M. Asharaf, N. Zarokanellos, I. Hoteit, Factors governing the deep ventilation of the Red Sea. *J. Geophys. Res.* **120**, 7493–7505 (2015).

19. J. Marshall, F. Schott, Open-ocean convection: Observations, theory, and models. *Rev. Geophys.* **37**, 1–64 (1999).

20. S. Legg, B. Briegleb, Y. Chang, E. P. Chassignet, G. Danabasoglu, T. Ezer, A. L. Gordon, S. Griffies, R. Hallberg, L. Jackson, W. Large, T. M. Özgökmen, H. Peters, J. Price, U. Riemenschneider, W. Wu, X. Xu, J. Yang, Improving oceanic overflow representation in climate models: The Gravity Current Entrainment Climate Process Team. *Bull. Am. Meteorol. Soc.* **90**, 657–670 (2009).

21. G. Stenchikov, A. Robock, V. Ramaswamy, M. Daniel Schwarzkopf, K. Hamilton, S. Ramachandran, Arctic Oscillation response to the 1991 Mount Pinatubo eruption: Effects of volcanic aerosols and ozone depletion. *J. Geophys. Res. Atmos.* **107**, 4803 (2002).

22. G. Stenchikov, T. L. Delworth, V. Ramaswamy, R. J. Stouffer, A. Wittenberg, F. Zeng, Volcanic signals in oceans. *J. Geophys. Res. Atmos.* **114**, D16104 (2009).

23. O. H. Otterå, M. Bentsen, H. Drange, L. Suo, External forcing as a metronome for Atlantic multidecadal variability. *Nat. Geosci.* **3**, 688–694 (2010).

24. D. Swingedouw, P. Ortega, J. Mignot, E. Guilyardi, V. Masson-Delmotte, P. G. Butler, M. Khodri, R. Séférian, Bidecadal North Atlantic ocean circulation variability controlled by timing of volcanic eruptions. *Nat. Commun.* **6**, 6545 (2015).

25. T. L. Delworth, F. Zeng, G. A. Vecchi, X. Yang, L. Zhang, R. Zhang, The North Atlantic Oscillation as a driver of rapid climate change in the Northern Hemisphere. *Nat. Geosci.* **9**, 509–512 (2016).

26. A. J. Simmons, P. Poli, D. P. Dee, P. Berrisford, H. Hersbach, S. Kobayashi, C. Peubey, Estimating low-frequency variability and trends in atmospheric temperature using ERA-Interim. *Q. J. R. Meteorol. Soc.* **140**, 329–353 (2014).

27. D. P. Dee, S. Uppala, Variational bias correction of satellite radiance data in the ERA-Interim reanalysis. *Q. J. R. Meteorol. Soc.* **135**, 1830–1841 (2009).

28. A. Köhl, D. Stammer, Variability of the meridional overturning in the North Atlantic from the 50-year GECCO state estimation. *J. Phys. Oceanogr.* **38**, 1913–1930 (2008).

29. J. Hansen, R. Ruedy, M. Sato, K. Lo, Global surface temperature change. *Rev. Geophys.* **48**, RG4004 (2010).

Citation: F. Yao, I. Hoteit, Rapid Red Sea Deep Water renewals caused by volcanic eruptions and the North Atlantic Oscillation. *Sci. Adv.* **4**, eaar5637 (2018).

Science Advances

Rapid Red Sea Deep Water renewals caused by volcanic eruptions and the North Atlantic Oscillation

Fengchao Yao and Ibrahim Hoteit

ARTICLE TOOLS	http://advances.sciencemag.org/content/4/6/eaar5637
SUPPLEMENTARY MATERIALS	http://advances.sciencemag.org/content/suppl/2018/06/25/4.6.eaar5637.DC1
REFERENCES	This article cites 28 articles, 1 of which you can access for free http://advances.sciencemag.org/content/4/6/eaar5637#BIBL
PERMISSIONS	http://www.sciencemag.org/help/reprints-and-permissions

Use of this article is subject to the Terms of Service